Physica Medica 64 (2019) 188–194

Contents lists available at ScienceDirect

Physica Medica

journal homepage: www.elsevier.com/locate/ejmp

Original paper

Feasibility of clinical electron beam formation using polymer materials produced by fused deposition modeling

Irina Miloichikova[a,b,*], Angelina Bulavskaya[a], Yury Cherepennikov[a], Boris Gavrikov[c], Elisabetta Gargioni[d], Dmitrij Belousov[e], Sergei Stuchebrov[a]

[a] National Research Tomsk Polytechnic University, Lenina Avenue 30, 634050 Tomsk, Russia
[b] Cancer Research Institute of Tomsk NRMC RAS, Kooperativny Street 5, 634050 Tomsk, Russia
[c] Moscow City Oncology Hospital №62, Istra 27, 143423 Moscow, Russia
[d] University Medical Center Hamburg-Eppendorf, Martinistrasse 52, 20246 Hamburg, Germany
[e] Institute of Automation and Electrometry SB RAS, Academician Koptyug Avenue 1, 630090 Novosibirsk, Russia

ARTICLE INFO

Keywords:
Electron beam
Fused deposition modeling
Radiation therapy
ABS and HIPS plastics

ABSTRACT

The main challenge in electron external beam radiation therapy with clinical accelerators is the absence of integrated systems to form irregular fields. The current approach to provide conformal irradiation is to use additional metallic shaping blocks, with inefficient and expensive workflows. This work presents a simple method to form therapeutic electron fields using 3D printed samples. These samples are manufactured by fused deposition modeling, which can affect crucial properties, such as material homogeneity, due to the presence of residual air-filled cavities. The applicability of this method was therefore investigated with a set of experiments and Monte Carlo simulations aimed at determining the electron depth dose distribution in polymer materials. The results show that therapeutic electron beams with energies 6–20 MeV can be effectively absorbed using these polymeric samples. The model developed in this study provides a way to assess the dose distribution in such materials and to calculate the appropriate thickness of polymer samples for therapeutic electron beam formation. It is shown that for total absorption of 6 MeV electron beams the material thickness should be at least 4 cm, while this value should be at least 8 cm for 12 MeV and 11 cm for 20 MeV, respectively. The results can be used to further develop 3D printing procedures for medical electron beam profile formation, allowing the creation of a collimator or absorber with patient-specific configuration using rapid prototyping systems, thus contributing to improve the accuracy of dose delivery in electron radiotherapy within a short manufacturing time.

1. Introduction

Fighting cancer remains an important issue in our modern society. According to the World Health Organization, the number of new cases per year was 14 million in 2012 and is projected to reach 21.6 million by 2030 [1]. In addition, the latest data show a global increase in pediatric cases of about 13% over the last two decades [2].

Currently, the effectiveness of cancer treatment is based on efficiency, safety, and comprehensiveness of the used approach, which includes a combination of modern technologies with basic treatment methods such as radiotherapy, surgery, and chemotherapy [3–5]. External beam radiotherapy accounts for almost 90% of cancer treatments that use ionizing radiation [4,6].

In particular, high-energy electron beams are extensively employed to this purpose due to the fact that electron interactions with matter allow for a high energy deposition in the tumor volume with steep energy deposition gradients in the surrounding and deep-lying normal tissues. Typically, clinical linear accelerators generate electron beams with energies in the range 4–20 MeV, which are suitable for treating superficial and shallow-lying lesions with depths of up to 6 cm [3,7,8].

Modern radiotherapy techniques allow for the delivery of a high single-time dose directly to the target volume [7]. Consequently, in order to ensure treatment accuracy and precision, strict requirements need to be met regarding the different parameters of radiotherapy, such as the absorbed dose to the target volume and the spatial profiles of therapeutic beams. Like for photon therapy, methods for modulating electron beams should therefore be further developed to ensure a better sparing of healthy tissue. Such methods should allow one to control

* Corresponding author at: National Research Tomsk Polytechnic University, Lenina Avenue 30, 634050 Tomsk, Russia.
E-mail address: miloichikova@tpu.ru (I. Miloichikova).

https://doi.org/10.1016/j.ejmp.2019.07.014
Received 7 May 2019; Received in revised form 17 July 2019; Accepted 17 July 2019
Available online 23 July 2019

relevant field characteristics, such as depth dose distribution, transverse beam profile, and beam divergence.

Collimation is one of the most widely used approaches for electron beam formation and modulation. Due to the high amount of electron scattering in air, additional applicators are typically attached to the accelerator head for field shaping. The front edge of such applicators is usually situated 5 cm from the patient's body surface when treating in a standard geometry with a source-to-surface distance of 100 cm [7]. The short distance between front edge and patient surface prevents high broadening of the electron beam sizes due to scattering in air, thus allowing for the delivery of radiation fields with the given shape [8]. Clinical radiation sources are usually equipped with standard sets of apertures and metal blocks that only allow for the formation of fixed-shaped fields with predetermined manufacturer sizes, thus delivering uniform dose distribution in the target volume [9]. This limited number of field sizes and the complex block manufacturing are therefore not suitable for the formation of arbitrary beams with complex shapes, which are often needed to ensure a better conformity of radiotherapy treatments. Moreover, the necessity to manually set these units by the operator for each irradiation session increases the preparation time for treatment, while the human factor introduces additional errors in the accuracy of dose delivery.

Another, more flexible method to form individualized electron field shapes is to use multileaf collimators (MLCs). Only a few studies have investigated the possibility of using conventional photon MLC for electron radiotherapy with intensity modulation, such as modulated electron radiotherapy (MERT). For this case, a significant reduction of the air gap between the patient's body and the treatment head, which should not be more than 30 cm [10–12], was found to be necessary. This limits the beam incidence angle to avoid dangerous collisions during gantry rotation [12].

There are also several studies on therapeutic electron beam formation connected with special add-on MLCs, which are fixed by clamping frames to the head of the accelerator and located close to the patient's body surface (up to 10 cm). For example, a simplified collimator, called few leaf electron collimator, comprising four motorized plates, has been developed for radiotherapy with intensity modulation by rectangular electron beams [13], while other groups have developed various MLC prototypes for irregular electron beams (eMLC) [14–16]. Some disadvantages in using these collimators are, however, their large size and weight (more than 30 kg), the necessity to place the leaf motors close to the patient's body, difficulties in ensuring the quality of the leaf displacement system and dose delivery, and the limitation of their use to vertical beam incidence as far as the gantry rotation leads to the eMLC's fixing frame deflection [13–16]. Another issue that needs to be considered in electron radiotherapy with intensity modulation is the requirement for accurate algorithms for dose calculation, such as those based on the Monte Carlo method, with a significant computing time as a consequence [12,17–18].

Currently, both approaches using built-in and additional MLC are at the stage of experimental research and not widely used in routine clinical practice.

Considering all above-mentioned difficulties, the less flexible use of individual collimators is widely considered to be the most practical method, despite the fact that shaping blocks are usually produced by cutting or casting of special metal alloys [9] including metals such as cadmium, bismuth, and lead [19]. This causes the release of toxic vapors from metal alloys, high cost of equipment, intricate requirements for safety personnel qualification, and time-consuming production. Therefore, it would be desirable to improve this procedure, for example by using less toxic materials and cost-effective production techniques.

Current 3D printing technologies allow for high accuracy and quality manufacturing and are widely used in various areas, including medicine [20]. The rapid and simple process of 3D polymer printing for use in modern devices has been shown to be advantageous over methods based on the use of metal. In particular, several recent studies are dedicated to beam energy modulation with 3D printing [21–28]. These studies show the efficiency of 3D printed samples for external beam radiotherapy with photon, proton and electron beams [21–25] and contact gamma radiotherapy [23,26,27]. Moreover, it has been demonstrated that plastics can be used to make forming elements for electron beams during external beam radiotherapy sessions [28].

Given the potential of 3D printing for individually configuring radiation beams and providing a prompt and high-quality solution of clinical problems (such as individual field shaping or bolus and compensator formation), an alternative approach of clinical electron field formation using polymer objects produced by 3D printing was developed in this study. The depth dose distributions of clinical electron beams in acrylonitrile butadiene styrene (ABS) and high-impact polystyrene (HIPS) plastics were measured with radiochromic films. Moreover, a simple model to simulate the electron beam dose distribution in polymer samples for fast determination of the block thickness for appropriate beam attenuation was created using the GEANT4 toolkit [29–30]. Finally, the results of the model are compared with experimental data.

2. Materials and methods

2.1. Polymer materials

Owing to a wide variety of polymer materials suitable for creating objects using the rapid prototyping technique [31], it is necessary to carefully study their properties and infer their suitability to be used as field-forming elements for electron dose delivery. In particular, the electron depth-dose distribution inside the material must be known to define the polymer's sample thickness that is necessary to partially or totally absorb electron beams depending on the predetermined task of dose distribution and beam profile forming.

ABS and HIPS plastics are considered the most suitable polymeric materials for this purpose due to their low cost, high availability, and favorable mechanical properties [31]. The sets of plate samples, with various thicknesses, made of ABS or HIPS plastic produced by Bestfilament (Bestfilament, Tomsk, Russian Federation) [32] (Fig. 1) were manufactured by fused deposition modeling and used for investigating depth dose distributions. The thickness of each was chosen for measuring the depth dose distribution with 1-mm spatial resolution. The rapid prototyping device "UP! Plus 2" by Tiertime (Beijing Tiertime Technology Co., Beijing, China) [33] was used in this work to create the samples.

The polymer plate samples were lightly ground after manufacturing to ensure the highest possible smoothness while the thickness was controlled to be close to its nominal value.

2.2. Clinical linear electron accelerators

The depth dose distributions of clinical electron beams in the polymer samples made of ABS and HIPS plastics as mentioned above were first obtained experimentally. Measurements were carried out for the electron beams of two different electron linear accelerators. The

Fig. 1. Appearance of plate samples made of ABS (red) and HIPS (white) plastics.

first is an ONCOR Impression Plus therapeutic linear accelerator by Siemens (Siemens, Oncology Care Systems, Germany), with an energy range of 6–18 MeV, mounted at the Moscow City Oncology Hospital №62 (Moscow, Russia) [34]. The second is a TrueBeam 2.0 by Varian (Varian Medical Systems Inc., Palo Alto, California, United States) from the University Medical Center Hamburg-Eppendorf (UKE, Hamburg, Germany) [35], with an energy range of 6–20 MeV.

2.3. Depth-dose measurements

GafChromic EBT3 (Ashland Inc., Covington, Kentucky, United States) dosimetry films were used in this study for analyzing the spatial distribution of electron beams [34]. The advantage of using films with respect to other detectors types, such as ionization chambers, thermoluminescent dosimeters, or semiconductor dosimeters, is the ability to simultaneously obtain planar dose distributions [36,37].

The films were first calibrated according to international recommendations [37]. The calibration procedure was carried out using a 12-MeV electron beam at the clinical linear electron accelerator ONCOR Impression Plus [34]. The calibration curve was obtained in the dose range 0.1–10.0 Gy by sequential irradiation of GafChromic EBT3 film samples. A colored flatbed scanner Epson Perfection V750 Pro was used to digitize the films [38], that were scanned in 48-bit color mode with 72-dpi spatial resolution, which corresponds to a 0.35-mm pixel size. The resulting digital images were saved in TIFF format and analyzed using an *ad-hoc* program code written in MATLAB [39]. A predetermined region of interest with $1 \times 1\ cm^2$ size located in the film's central part was used for the analysis [40,41].

Some studies have shown that the maximum uncertainty in the pure optical density determination associated with film inhomogeneity is about 5% [40,42]; this value is therefore considered to be the maximum uncertainty in the electron dose measurements performed during this work. The measured calibration curve was then used to analyze the spatial distribution of the electron beam dose in the polymer samples.

2.4. Experimental geometry

The experiments were carried out using the following set-up: source to plastic surface distance: 100 cm; field size: $10 \times 10\ cm^2$, formed by a standard metal applicator with square collimation window of this size; angle between electron beam and plastic samples: 90°. The radiation dose was 1 Gy at the dose maximum in water (100 MU) for all given nominal electron energies.

The GafChromic EBT3 films were fixed between the tightly pressed polymer plate samples and located at the radiation field's central part parallel to the electron beam propagation plane. A schematic view of the experimental set-up is shown in Fig. 2.

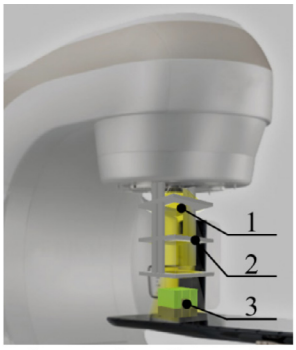

1 – electron beam; 2 – metal applicator; 3 – polymer absorber

Fig. 2. Schematic geometry of the experiment to determine the electron beam depth dose distribution in a polymer material.

2.5. Monte Carlo simulation

The Monte Carlo method was used to calculate the absorbed dose, as this method has been shown in several investigations to accurately simulate the interactions of an electron beam for radiotherapy tasks [43,44]. In this study, a simple computational model was developed using the GEANT4 toolkit (version 10.2p02) [45–47]. GEANT4 is provided with the following electromagnetic physics models – standard (1 keV–100 TeV), Livermore (250 eV–100 GeV), Penelope (100 eV–1 GeV), Geant4-DNA (4 eV–400 MeV) [45,47–50]. In our model, we used QBBC physics list, which is recommended for medical physics simulations [51]. This physics list is based on GEANT4 standard electromagnetic physics package, which correctly describes electromagnetic processes for the 1 keV to 100 TeV energy region [47,48,51]. The electron propagation in GEANT4 is described by a condensed history algorithm and based on the Lewis theory, providing information about the moment, the angular, and the spatial displacement of the particles. The package considers Bremsstrahlung and ionization processes for electrons in Möller scattering. An analytical approach combines numerical databases with analytical cross-section models. Atomic electrons are considered "quasi free" (the binding energy is accounted for in the case of photoelectric effect only), while the nucleus is fixed. This package does not include Rayleigh scattering and atomic relaxation processes [45–51].

In the simulation, the electron source was considered to have transverse dimensions of $10 \times 10\ cm^2$ and a uniform particle distribution over the surface. The source was located at a distance of 1 mm from the surface of the polymer absorber with a size of $30 \times 30 \times 30\ cm^3$, as schematically shown in Fig. 3. The depth-dose distribution was calculated along the central axis of the electron beam, with a voxel size of $4.75 \times 4.75 \times 1\ mm^3$. The number of primary particle histories was 10^8. The statistical error for the calculated results of the simulation was less than 1%.

Since the real clinical electron beam is not mono-energetic, the average energy value on the water phantom surface was determined for each nominal energy in accordance with international recommendations for clinical dosimetry [52–54]. The calculated values of the average energy for nominal electron beam energies of 6, 12, 18, and 20 MeV resulted to be 5.3, 10.8, 17.8, and 18.8 MeV, respectively. These values were obtained for the considered therapeutic linear accelerators based on clinical dosimetry data. A Gaussian distribution with standard deviation $\sigma = 3\%$ and mean values as calculated from above was then used to specify the electron beam energy in the simulations.

Table 1 shows the main parameters of the ABS and HIPS plastics manufactured by Bestfilament that were used in this model [55,56]. Note, however, that the exact formula and mass fraction of the chemical elements in the plastics are unknown and cannot be acquired, and hence, averaged parameter values, according to literature, were used in the simulations [31,57,58]. In the simulation the ABS and HIPS plastics is defined by mass fraction of chemical elements, material density and average excitation energy (Table 1).

Since manufacturing by fused deposition modeling implies a layer-by-layer construction of the object from thermoplastic, the actual density of the completed objects becomes lower than that of the raw material or filament [31]. To take this into account, the real density of the polymer plate samples was obtained by measuring their mass and volume. The density of the sample for ABS plastic was determined to be $0.90 \pm 0.06\ g/cm^3$ and that for HIPS plastic $0.88 \pm 0.07\ g/cm^3$, respectively.

The ESTAR database of the National Institute of Standards and Technologies (USA) [59] was used to determine the average excitation energy for ABS and HIPS plastics according to mass fraction of chemical elements and density required to create a model of each substance in the GEANT4 toolkit [46]. The average excitation energy characterizes the stopping properties of a medium. In ESTAR, these values are used

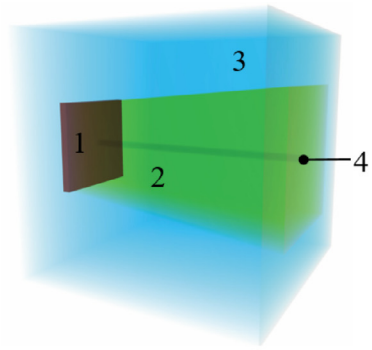

1 – electron source; 2 – electron beam; 3 – polymer absorber; 4 – calculated voxels

Fig. 3. Schematic simulation set-up.

Table 1
Parameters of the polymer materials used in the Monte Carlo simulation.

	ABS plastic	HIPS plastic
Molecular formula	$C_8H_8{\cdot}C_4H_6{\cdot}C_3H_3N$	C_8H_8
Mass fraction	Carbon – 84.68% Hydrogen – 7.93% Nitrogen – 7.39%	Carbon – 92.26% Hydrogen – 7.74%
Density	0.90 g/cm^3	0.88 g/cm^3
Average excitation energy	65.7 eV	65.9 eV

according to the ICRU Report 37 [60].

The simulation was used to calculate, in a fast and simple way, the electron dose distribution in the absorber volume and therefore could be used in the future for determining the appropriate material thickness in a given electron beam for a specific task. To confirm the reliability of the simulation, the calculated distributions were thus compared with those obtained experimentally.

3. Results and discussion

3.1. Analysis of the electron beam depth dose distribution in ABS and HIPS plastics

Fig. 4 shows examples of the depth dose distributions in ABS plastic for electron beams with nominal energies of 6 and 12 MeV that were measured at the True Beam of the UKE.

The percent depth dose distribution (PDD) along the central axis of the beam was also determined by averaging over the five neighboring lines (1.8 mm) to reduce the contribution of errors caused by possible film defects, such as scratches and local inhomogeneities. Fig. 5a shows the obtained PDDs of electron beams in ABS plastic with nominal energies of 6, 12, and 20 MeV. Fig. 5b shows the measured depth dose distributions in HIPS plastic samples that were performed at the Moscow City Oncology Hospital №62 for nominal electron beam energies of 6, 12, and 18 MeV.

Fig. 5a shows that in ABS plastic the total absorption of electron beams with nominal energies of 6, 12, and 20 MeV occurs at layer thicknesses of 4.0, 7.5, and 10.5 cm (R_{max}), respectively. Fig. 5b shows that in HIPS plastic, total absorption of electron beams with nominal energies of 6, 12, and 18 MeV occurs at layer thicknesses of 4.0, 8.0, and 11.0 cm, respectively.

The obtained distributions follow a typical curve for an electron beam in a tissue-equivalent medium. However, for small depths, the distribution is atypical, most probably due to the film edge deformation during cutting and the presence of an air gap between the polymer plate samples and the film, which technically cannot be eliminated without creating an obstacle for the primary electron beam [61,62].

3.2. Comparison of the experimental and simulated depth dose distributions

To make better sense of the experimental data, the percentage depth dose (PDD) distributions in water, which were measured for both accelerators according to the internal guidelines for clinical dosimetry [62] are compared in Fig. 6 for nominal energies of 6 and 12 MeV; the standard conditions used for both accelerators were a source-to-surface distance of 100 cm and a radiation field of 10 × 10 cm^2.

Fig. 6 shows that the PDDs in water for the two accelerators are in good agreement. Deviations in the absorbed dose maximum position (d_{max}) and the depth corresponding to 50% of the dose maximum value (R_{50}) are less than 2 mm. The latter means that it is possible to qualitative compare the obtained data for the polymer samples for different clinical accelerators (Fig. 5).

A comparison of the PDDs of electron beams in ABS and HIPS

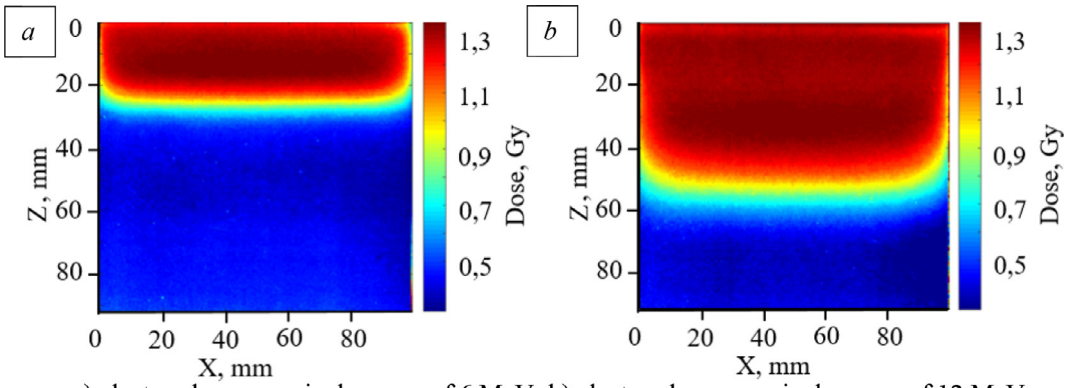

a) electron beam nominal energy of 6 MeV; b) electron beam nominal energy of 12 MeV

Fig. 4. Experimental depth dose distributions of electron beams in ABS plastic with nominal energies of 6 and 12 MeV.

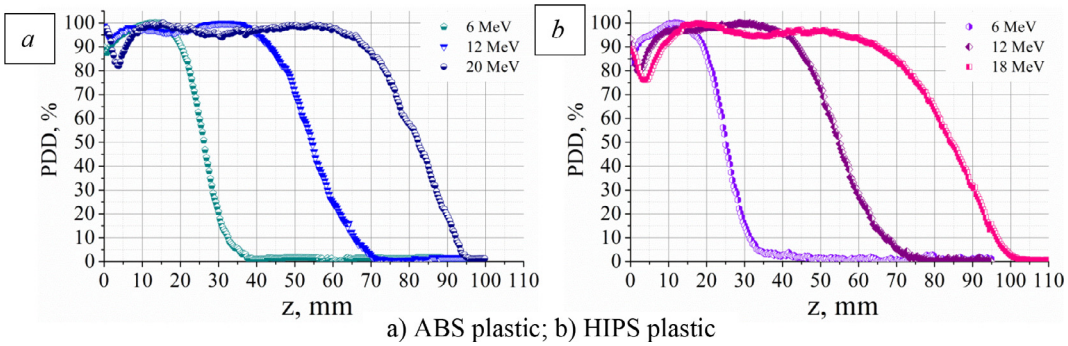

Fig. 5. Experimental PDDs of electron beams in ABS and HIPS plastics plastic.

plastics for energies of 6 and 12 MeV is shown in Fig. 7. The obtained data show that the PDDs for the two polymer materials are in good agreement, which improves at higher energies.

Figs. 8 and 9 compare the experimental and simulated PDDs for electron beam energies of 6.0 MeV (simulated average energy is 5.3 MeV, σ = 3%) and 12.0 MeV (simulated average is 10.8 MeV, σ = 3%). Note that the results for other electron beam energies follow the same trends as those shown in Figs. 8 and 9.

As seen from the obtained distributions, the simulated data using a simple model are appropriate to capture the behavior of the electron beams in both polymer materials in the region behind the d_{max}. Note, however, that at depths greater that about 6 cm the measured dose was higher than in simulations, which is due to the presence of bremsstrahlung generated by the electrons in structural elements of treatment head in the physical experiment. In the simulation, we do not observe the part of this bremsstrahlung as far as we use simplified model of the forming system accounting not every element of the treatment head. Such radiation is generated from the interaction of electrons with the accelerator collimating system and the medium, which is either the patient's body or the phantom (like in this study). According to preliminary estimations, the bremsstrahlung contribution to the dose exposure for modern accelerators is between 0.5% and 5.0% for an electron beam with nominal energies in the range 6–20 MeV [9].

The difference in the experimental and simulated PDDs at the entrance of the polymer phantom can be explained by the simplifications employed in the model, wherein the contribution of the secondary radiation generated in the accelerator therapeutic head elements is unaccounted for. The shift in the location of the maximum of the experimental curves to a region of smaller depths and the difference in the absorbed dose value up to the maximum region are caused by both secondary radiation contributions and the presence of an air gap between the polymer plate samples and the dosimetry films. Note that completely removing the air in this gap is technically unachievable because any additional fixing device in the beam path would cause deformations. On the other hand, the relatively rough surface of the polymer samples produced by fused deposition modeling also affects the obtained results; additional grinding also does not result in an ideal surface without changing the plate thickness.

The results in Figs. 8 and 9 demonstrate that the simple Monte Carlo model is accurate enough for the determination of the minimum thickness necessary to absorb electron beams with energies in the range of 6–20 MeV, which can be helpful in the future to develop ABS and HIPS collimating devices without performing complex and time-consuming experiments.

The comparison of the simulation results with CSDA ranges from NIST database [59] for both considered plastics shows simulation adequacy. Thus extrapolated ranges of electrons (R_{ex}) for 6 and 12 MeV nominal energies (E_e) calculated with simulated data is close to corresponding CSDA ranges (Table 2). On the other hand, we can say, that these values cannot be used as collimators thicknesses, as far as do not provide total dose absorption for primary and secondary radiation. Therefore, the collimators thicknesses should be chosen with simulated depth dose distributions in range where the dose value close to zero (R_{max}).

The observed data shows high efficiency of the electron beam absorption by ABS and HIPS plastic produced with rapid prototyping. This proves the possibility to use both considered materials for producing and 3D printed samples for total absorption of electron beams with typical clinical accelerators energies ranging from 6 to 20 MeV.

4. Conclusion

In this study, the interaction of accelerated electron beams with ABS and HIPS plastics manufactured by fused deposition modeling was considered for dosimetric purposes in a typical therapeutic situation. The study included a simple Monte Carlo simulation of the behavior of megavoltage electrons in polymers and an experimental investigation using medical accelerators.

The Monte Carlo model provides an effective simulation of electron beams in ABS and HIPS plastics with nominal energies in the range

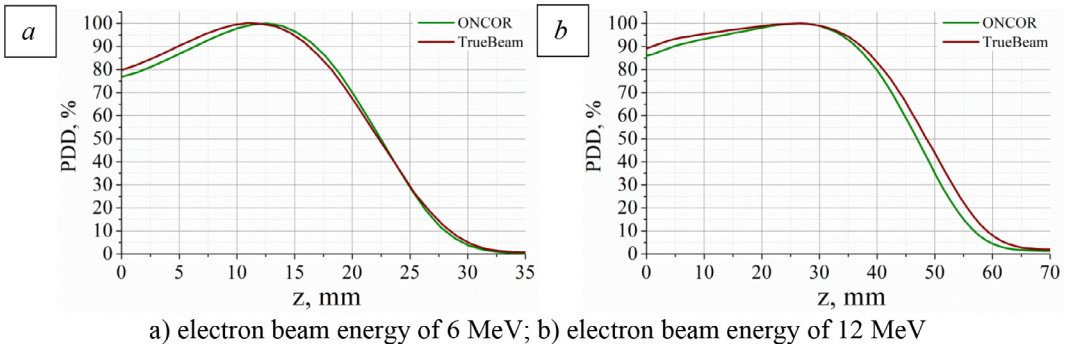

Fig. 6. Experimental PDDs of electron beams in water phantom with nominal energies of 6 and 12 MeV for the TrueBeam 2.0 and ONCOR Impression Plus accelerators.

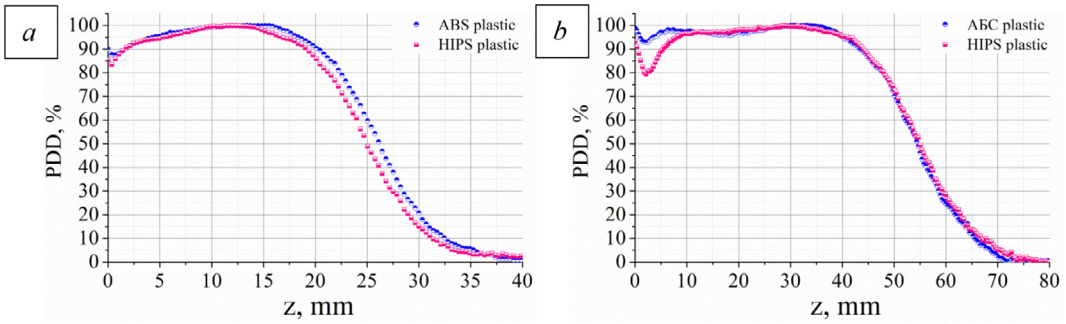

Fig. 7. Experimental PDDs of electron beams in ABS and HIPS plastic with nominal energies of 6 and 12 MeV.

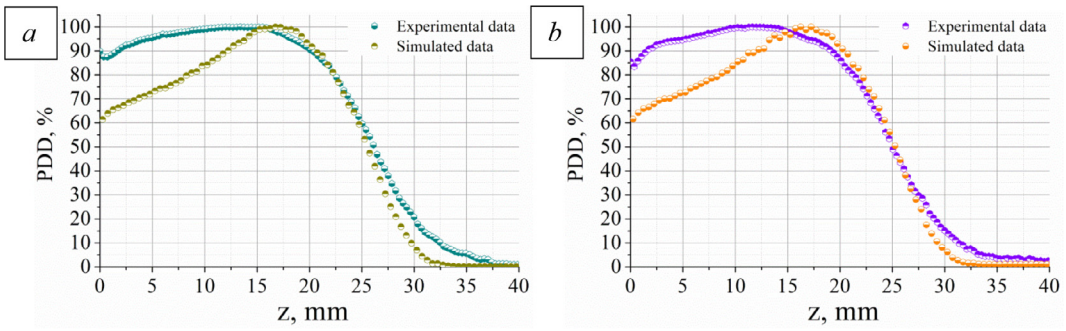

Fig. 8. Experimental and simulated PDDs of electron beams in ABS and HIPS plastics with nominal energy of 6 MeV.

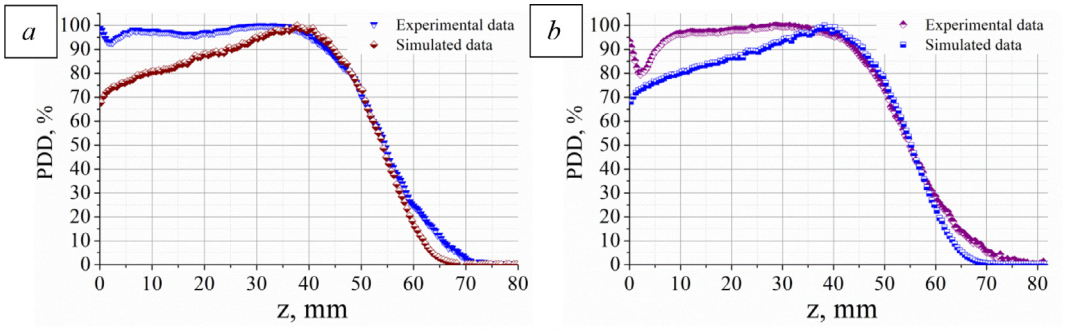

Fig. 9. Experimental and simulated PDDs of electron beams in ABS and HIPS plastics with nominal energy of 12 MeV.

Table 2
Comparison of Monte Carlo simulation results with CSDA range.

	Nominal E_e, MeV	R_{ex}, cm	R_{max}, cm	CSDA range, cm
ABS plastic	6	3.1	4.0	3.1
	12	6.2	7.5	6.1
HIPS plastic	6	2.9	4.0	3.2
	12	6.3	8.0	6.3

6–20 MeV. Specifically, the model was able to accurately describe the electron beam depth dose distribution in the region behind the absorption maximum. In the future, the model can therefore be applied to determine the minimum thickness of polymer samples necessary to form therapeutic electron fields, particularly for beam collimation.

The experimental investigation also showed that plastic samples manufactured by fused deposition modeling contain air cavities, which affect the interaction processes with radiation. Hence, in future work, additional corrections must be included in the Monte Carlo model to account for this factor.

The simulated and experimental results showed that the total absorption of clinical electron beams with nominal energies of 6, 12, and 20 MeV in ABS plastic occurs at layer thicknesses of 4.0, 7.5, and 10.5 cm, respectively. Similarly, the total absorption of electron beams with nominal energies of 6, 12, and 18 MeV in HIPS plastic occurs at layer thicknesses of 4.0, 8.0, and 11.0 cm, respectively. These values do not exceed the geometric limits of accelerator forming elements. These results also demonstrate that the electron absorption in these plastic samples is sufficient to collimate therapeutic beams and therefore to substitute metal alloys for beam shaping. Furthermore, the results provide opportunities to further develop this method for medical electron beam formation, creating a collimator, bolus or compensator with patient-specific configuration using rapid prototyping technologies, which can help to improve the accuracy of electron radiotherapy procedures in a cost-effective way and with a short manufacturing time.

Acknowledgment

This work was supported by the Russian Science Foundation, project

No. 18-79-10052.

References

[1] International Agency for Research on Cancer. Press Release N° 224 Global Battle Against Cancer Won't be Won with Treatment Alone. Effective Prevention Measures Urgently Needed to Prevent Cancer Crisis 2014, https://www.iarc.fr/en/media-centre/pr/2014/pdfs/pr224_E.pdf; 2014 [accessed 16 April 2019].

[2] International Agency for Research on Cancer. Press Release N° 251 Latest data show a global increase of 13% in childhood cancer incidence over two decades 2017, https://www.iarc.fr/en/media-centre/pr/2017/pdfs/pr251_E.pdf; 2017 [accessed 16 April 2019].

[3] Bernier J, Hall EJ, Giaccia A. Radiation oncology: a century of achievements. Nat Rev Cancer 2004;4(9):737–47. https://doi.org/10.1038/nrc1451.

[4] Gerber DE, Chan TA. Recent advances in radiation therapy. Am Fam Physician 2008;78(11):1254–62. https://doi.org/10.1186/1741-7015-8-25.

[5] Lee CD. Recent developments and best practice in brachytherapy treatment planning. Brit J Radiol 2014;87(1041):20140146. https://doi.org/10.1259/bjr.20140146.

[6] Garibaldi C, et al. Recent advances in radiation oncology. Ecancermedicalscience 2017;11:785. https://doi.org/10.3332/ecancer.2017.785.

[7] Hogstrom KR, Almond PR. Review of electron beam therapy physics. Phys Med Biol 2006;51(13):R455. https://doi.org/10.1088/0031-9155/51/13/R25.

[8] Thwaites DI, Tuohy JB. Back to the future: the history and development of the clinical linear accelerator. Phys Med Biol 2006;51(13):R343. https://doi.org/10.1088/0031-9155/51/13/R20.

[9] Khan FM, Gibbons JP. Khan's the physics of radiation therapy. Lippincott Williams & Wilkins; 2014.

[10] Mueller S, et al. Electron beam collimation with a photon MLC for standard electron treatments. Phys Med Biol 2018;63(2):025017https://doi.org/10.1088/1361-6560/aa9fb6.

[11] Henzen D, et al. Beamlet based direct aperture optimization for MERT using a photon MLC. Med Phys 2014;41(12):121711https://doi.org/10.1118/1.4901638.

[12] Lloyd SAM, et al. Validation of Varian TrueBeam electron phase–spaces for Monte Carlo simulation of MLC shaped fields. Med Phys 2016;43(6 Part 1):2894–903. https://doi.org/10.1118/1.4949000.

[13] Al-Yahya K, et al. Energy modulated electron therapy using a few leaf electron collimator in combination with IMRT and 3D-CRT: Monte Carlo-based planning and dosimetric evaluation. Med Phys 2005;32(9):2976–86. https://doi.org/10.1118/1.2011089.

[14] Hogstrom KR, et al. Dosimetry of a prototype retractable eMLC for fixed beam electron therapy. Med Phys 2004;31(3):443–62. https://doi.org/10.1118/1.1644516.

[15] Nassiri M, et al. TH-C-AUD-05: Monte Carlo simulation and measurement investigations of motorized multi-leaf collimator for electron beam delivery. Med Phys 2007;34:2627. https://doi.org/10.1118/1.2761664.

[16] Eldib AA, et al. Dosimetric characteristics of an electron multileaf collimator for modulated electron radiation therapy. J Appl Clin Med Phys 2010;11(2):5–22. https://doi.org/10.1120/jacmp.v11i2.2913.

[17] Henzen D, et al. Monte Carlo based beam model using a photon MLC for modulated electron radiotherapy. Med Phys 2014;41(2):021714https://doi.org/10.1118/1.4861711.

[18] Klein EE, et al. Validation of calculations for electrons modulated with conventional photon multileaf collimators. Phys Med Biol 2008;53(5):1183–208. https://doi.org/10.1088/0031-9155/53/5/003.

[19] PAR Scientific A/S ACD-4 mk 5 block cutting unit, http://www.parscientific.com/Acd4mk5.html; 2016 [accessed 16 April 2019].

[20] Liaw CY, Guvendiren M. Current and emerging applications of 3D printing in medicine. Biofabrication 2017;9(2):024102https://doi.org/10.1088/1758-5090/aa7279.

[21] Su S, Moran K, Robar JL. Design and production of 3D printed bolus for electron radiation therapy. J Appl Clin Med Phys 2014;15(4):194–211. https://doi.org/10.1120/jacmp.v15i4.4831.

[22] Burleson S, et al. Use of 3D printers to create a patient-specific 3D bolus for external beam therapy. J Appl Clin Med Phys 2015;16(3):166–78. https://doi.org/10.1120/jacmp.v16i3.5247.

[23] Zhao Y, et al. Clinical applications of 3-dimensional printing in radiation therapy. Med Dosim 2017;42(2):150–5. https://doi.org/10.1016/j.meddos.2017.03.001.

[24] Zou W, et al. Potential of 3D printing technologies for fabrication of electron bolus and proton compensators. J Appl Clin Med Phys 2015;16(3):90–8. https://doi.org/10.1120/jacmp.v16i3.4959.

[25] Łukowiak M, et al. Utilization of a 3D printer to fabricate boluses used for electron therapy of skin lesions of the eye canthi. J Appl Clin Med Phys 2017;18(1):76–81. https://doi.org/10.1002/acm2.12013.

[26] Harris BD, Nilsson S, Poole CM. A feasibility study for using ABS plastic and a low-cost 3D printer for patient-specific brachytherapy mould design. Australas Phys Eng Sci Med 2015;38(3):399–412. https://doi.org/10.1007/s13246-015-0356-3.

[27] Cunha JAM, et al. Evaluation of PC ISO for customized, 3D printed, gynecologic 192Ir HDR brachytherapy applicators. J Appl Clin Med Phys 2015;16(1):246–53. https://doi.org/10.1120/jacmp.v16i1.5168.

[28] Miloichikova IA, et al. Formation of electron beam fields with 3D printed filters. AIP Conf Proc 2016;1772:060018https://doi.org/10.1063/1.4964598.

[29] Miloichikova IA, et al. Analysis of plane-parallel electron beam propagation in different media by numerical simulation methods. Russ Phys J 2018;60(12):2115–22. https://doi.org/10.1007/s11182-018-1334-5.

[30] Stuchebrov SG, et al. Numerical simulation of the microtron electron beam absorption by the modified ABS-plastic. J Phys Conf Ser 2016;671:012036https://doi.org/10.1088/1742-6596/671/1/012036.

[31] France AK. Make: 3D printing: the essential guide to 3D printers. Maker Media, Inc.; 2013.

[32] BESTFILAMENT Filaments manufacture, https://bestfilament.ru/en/; 2019 [accessed 16 April 2019].

[33] 3D printer «UP! Plus 2», https://www.up3d.com/up-plus-2/; 2018 [accessed 16 April 2019].

[34] ONCOR Digital Medical Linear Accelerator Specifications, http://www.siemens.com.tr/i/assets/saglik/onkoloji/oncor.pdf; 2009 [accessed 16 April 2019].

[35] The TrueBeam system, https://www.varian.com/sites/default/files/ resource_attachments/TrueBeamBrochure_RAD10119D_September2013.pdf; 2013 [accessed 16 April 2019].

[36] GafChromic EBT3, http://www.gafchromic.com/documents/EBT3_Specifications.pdf; 2014 [accessed 16 April 2019].

[37] Devic S, et al. Precise radiochromic film dosimetry using a flat-bed document scanner. Med Phys 2005;32(7 Part 1):2245–53. https://doi.org/10.1118/1.1929253.

[38] Epson Perfection V750 Pro. User's Guide, https://files.support.epson.com/pdf/prv7ph/prv7phug.pdf; 2015 [accessed 16 April 2019].

[39] MATLAB, https://uk.mathworks.com/products/matlab.html; 2018 [accessed 16 April 2019].

[40] Sipilä P, et al. Gafchromic EBT3 film dosimetry in electron beams energy dependence and improved film read-out. J Appl Clin Med Phys 2016;17(1):360–73. https://doi.org/10.1120/jacmp.v17i1.5970.

[41] Efficient Protocols for Accurate Radiochromic Film Calibration and Dosimetry, http://www.gafchromic.com/documents/Efficient%20Protocols%20for%20Calibration%20and%20Dosimetry.pdf; 2012 [accessed 16 April 2019].

[42] Devic S, et al. Dosimetric properties of improved GafChromic films for seven different digitizers. Med Phys 2004;31(9):2392–401. https://doi.org/10.1118/1.1776691.

[43] Rogers DWO. Fifty years of Monte Carlo simulations for medical physics. Phys Med Biol 2006;51(13):R287–301. https://doi.org/10.1088/0031-9155/51/13/R17.

[44] PRIMUS Basic Functional Description, Siemens ag medical solutions CS TSC2; 2003.

[45] Allison J, et al. Recent developments in Geant4. Nucl Instrum Meth Phys Res, Sect A 2016;835:186–225. https://doi.org/10.1016/j.nima.2016.06.125.

[46] Agostinelli S, et al. GEANT4 – a simulation toolkit. Nucl Instrum Meth Phys Res, Sect A 2003;506(3):250–303. https://doi.org/10.1016/S0168-9002(03)01368-8.

[47] Kyriakou I, et al. Microdosimetry of electrons in liquid water using the low-energy models of Geant4. J Appl Phys 2017;122(2). 024303-17.

[48] Collaboration G.E.A.N.T. et al. Physics reference manual. Version: geant4 2005;9(0):563.

[49] Yoriyaz H, et al. Physical models, cross sections, and numerical approximations used in MCNP and GEANT4 Monte Carlo codes for photon and electron absorbed fraction calculation. Med Phys 2009;36(11):5198–213. https://doi.org/10.1118/1.3242304.

[50] Low Energy Physics Lists https://twiki.cern.ch/twiki/bin/view/Geant4/LowePhysicsLists, 2018 [accessed 05 July 2019].

[51] QBBC http://geant4-userdoc.web.cern.ch/geant4-userdoc/UsersGuides/PhysicsListGuide/html/reference_PL/QBBC.html#pl-qbbc, 2018 [accessed 05 July 2019].

[52] Andreo P, et al. Absorbed dose determination in external beam radiotherapy: an international code of practice for dosimetry based on standards of absorbed dose to water. IAEA TRS 2000.

[53] Gerbi BJ, et al. Recommendations for clinical electron beam dosimetry: supplement to the recommendations of Task Group 25. Med Phys 2009;36(7):3239–79. https://doi.org/10.1118/1.3125820.

[54] Ding GX, Rogers DWO, Mackie TR. Mean energy, energy-range relationships and depth-scaling factors for clinical electron beams. Med Phys 1996;23(3):361–76. https://doi.org/10.1118/1.597788.

[55] ABS plastic Bestfilament, https://bestfilament.ru/abs-1-1.75-red/; 2018 [accessed 16 April 2019].

[56] HIPS plastic Bestfilament https://bestfilament.ru/hips-1-175-white-2/; 2018 [accessed 16 April 2019].

[57] Idemat (2003). Acrylonitrile Butadiene Styrene General Purpose, https://www.matbase.com/material-categories/natural-and-synthetic-polymers/thermoplastics/commodity-polymers/material-properties-of-acrylonitrile-butadiene-styrene-general-purpose-gp-abs.html#manufacturing-properties; 2003 [accessed 16 April 2019].

[58] Idemat (2003). High Impact Polystyrene General Purpose, https://www.matbase.com/material-categories/natural-and-synthetic-polymers/thermoplastics/commodity-polymers/material-properties-of-high-impact-polystyrene-hips.html#manufacturing-properties; 2003 [accessed 16 April 2019].

[59] Data basis ESTAR of National Institute of Standards and Technology, https://physics.nist.gov/PhysRefData/Star/Text/ESTAR-ut.html; 2018 [accessed 16 April 2019].

[60] ICRU Report 37, Stopping Powers for Electrons and Positrons. International Commission on Radiation Units and Measurements 1984.

[61] Jiang R, Kleer R, Piller FT. Predicting the future of additive manufacturing: a Delphi study on economic and societal implications of 3D printing for 2030. Technol Forecast Soc Change 2017;117:84–97. https://doi.org/10.1016/j.techfore.2017.01.006.

[62] Dutreix J, Dutreix A. Film dosimetry of high energy electrons. Ann N Y Acad Sci 1969;161(1):33–43. https://doi.org/10.1111/j.1749-6632.1969.tb34039.x.